INSTITUTE OF PHYSICS PUBLISHING JOURNAL OF PHYSICS B: ATOMIC, MOLECULAR AND OPTICAL PHYSICS

J. Phys. B: At. Mol. Opt. Phys. **34** (2001) 4455–4473 PII: S0953-4075(01)26310-X

Electron-impact excitation of Ne^{5+}

D M Mitnik[1], D C Griffin[1] and N R Badnell[2]

[1] Department of Physics, Rollins College, Winter Park, FL 32789, USA
[2] Department of Physics and Applied Physics, University of Strathclyde, Glasgow G4 0NG, UK

Received 2 July 2001, in final form 4 October 2001
Published 12 November 2001
Online at stacks.iop.org/JPhysB/34/4455

Abstract

We present the results of an 83-term, 180-level intermediate-coupling frame-transformation (ICFT) R-matrix close-coupling calculation of the electron-impact excitation of boron-like Ne^{5+}. All levels of the $2s^22p$, $2s2p^2$, $2p^3$, $2s^23\ell$, $2s^24\ell$, $2s2p3\ell$, $2p^23\ell$, 2s2p4s, 2s2p4p, and 2s2p4d configurations are included in the close-coupling expansion. This sizable calculation was performed using our new ICFT R-matrix codes designed for distributed-memory parallel computers. We compare our results from this calculation with those from our 11-term 20-level ICFT calculation and an earlier eight-term 15-level R-matrix calculation. Here we describe the nature of these calculations and present radiative rates and effective collision strengths for a selected number of the 16 110 transitions resulting from this work. The full set of data is available at the Oak Ridge National Laboratory Controlled Fusion Atomic Data Center Web site.

1. Introduction

Data for the electron-impact excitation of Ne ions are of importance in laboratory and astrophysical plasmas. In an earlier paper, we reported on large R-matrix close-coupling calculations for C-like Ne^{4+} [1]; in addition, we have recently completed work on F-like Ne^{+} [2]. In this paper, we present results from R-matrix close-coupling calculations of electron-impact excitation for B-like Ne^{5+}. Emission lines from this ion have been observed for transitions among the $n = 2$ levels in solar spectra and among the $n = 2$ and 3 levels in laboratory plasmas [3]. There have been two previous R-matrix close-coupling calculations of electron-impact excitation for this ion. The first was a ten-term LS calculation by Hayes [3]. In addition, Zhang *et al* [4], as part of a larger study of the B-like ions, performed an eight-term LS calculation and then transformed the resulting T-matrices to pure pair coupling so as to obtain effective collision strengths among the 15 $n = 2$ levels; however, they only provided data for transitions between the lowest seven levels.

Here we report on results from two R-matrix close coupling calculations for Ne^{5+} that employ the same Breit–Pauli configuration-interaction (CI) description of the target. The first was an 11-term, 20-level intermediate-coupling frame-transformation (ICFT) [5] R-matrix calculation that included the levels arising from the $2s^22p$, $2s2p^2$, $2p^3$ and $2s^23\ell$ configurations.

 © 2001 IOP Publishing Ltd Printed in the UK

The second was a much larger 83-term, 180-level ICFT calculation that included the levels arising from the $2s^22p$, $2s2p^2$, $2p^3$, $2s^23\ell$, $2s^24\ell$ $2s2p3\ell$, $2p^23\ell$, 2s2p4s, 2s2p4p, and 2s2p4d configurations. It was performed using our new parallel versions of the ICFT R-matrix codes.

The ICFT method is based on multi-channel quantum-defect theory (MQDT). One first employs MQDT to generate 'unphysical' K-matrices in pure LS coupling [6]. These matrices are then transformed to intermediate coupling using term-coupling coefficients and, finally, the physical K-matrices are determined from the unphysical K-matrices and the level energies using MQDT. This has been shown to avoid the problems associated with the term-coupling transformation of physical K-matrices, as is done in the program JAJOM [7], and yields results in excellent agreement with a full Breit–Pauli R-matrix calculation [5, 8].

Here we present our results for energy levels and dipole-radiative rates for selected transitions. In addition, we compare some of the collisional data obtained from our two calculations with each other and with the earlier results of Zhang *et al* [4]. The effective collision strengths for all 16 110 transitions between the 180 levels included in our largest calculation, as well as radiative rates for all dipole-allowed transitions, are available on the Internet at the Oak Ridge National Laboratory (ORNL) Controlled Fusion Atomic Data Center (CFADC)[3].

The remainder of this paper is organized as follows. In the next section, we give a brief description of the parallel implementation of our ICFT R-matrix codes. In section 3, we describe our structure and scattering calculations for this ion and, in section 4, we present our results for energies, radiative rates and collision strengths for selected transitions. In section 5, we provide a brief summary of our findings.

2. Parallel ICFT R-matrix codes

The 20-level ICFT R-matrix calculation was easily completed on one of our local workstations. However, even though the ICFT method is significantly faster than the full Breit–Pauli R-matrix method, calculations that include a large number of levels in the close-coupling expansion still require substantial time on a single processor. For example, our 138-level ICFT calculation on Ne^+ [2] required nearly two full weeks of run time on a workstation. For that reason, the 180-level calculation was carried out using the parallel version of these programs, the coding for which has just been completed. In this section, we provide a brief description of the parallel implementation of these codes.

The inner-region part of an ICFT R-matrix calculation, is performed using a modified version of the Queen's University of Belfast (QUB) RMATRX I suite of programs [9]. For calculations in LS coupling, it is divided into three stages. STG1 calculates the orbital basis and all radial integrals in the inner region and STG2 determines LS coupling matrix elements in the inner region. These two programs run quite efficiently as serial codes and have not been modified for parallel operation. STG3 (referred to as STGH in the RMATRX I package) reads the inner-region information from STG1 and STG2 and diagonalizes the continuum Hamiltonian. For large-scale calculations, the diagonalization of this $(N + 1)$-electron Hamiltonian is by far the most time consuming part of the inner-region operations. The time needed for the diagonalization of a matrix is proportional to N_r^3, where N_r is the rank of the matrix. For a typical calculation involving more than 80 terms, hundreds of different matrices up to a rank of $\approx 5 \times 10^3$ are diagonalized. Therefore, we wrote the parallel version of STG3 with an emphasis on distributing the diagonalization over the many processors of a distributed-memory parallel computer.

Using calls to the standard message-passing interface (MPI) library [10], the Hamiltonian matrix is directly partitioned over the processors. ScaLAPACK routines [11] are then used

[3] http://www-cfadc.phy.ornl.gov/data_and_codes.

for obtaining all eigenvalues and eigenvectors of the $(N + 1)$-electron Hamiltonian. The ScaLAPACK strategy is to perform as much of the calculation as possible by calls to the parallel basic linear algebra subprograms (PBLAS), provided by computer vendors (and others). The efficiency of ScaLAPACK software depends on the use of block-partitioned algorithms that provide the best load balancing with the maximum use of the PBLAS library on every processor. In addition to decreasing the time required for diagonalization, the partitioning of the Hamiltonian matrix also reduces memory requirements. The global Hamiltonian matrix is never constructed; only a local portion resides on each processor. In addition, global eigenvectors are not required, since partitioned eigenvectors are used to calculate the R-matrix surface amplitudes in parallel. There are a number of special features, such as the elimination of pseudo-resonances attached to states included in the CI expansion of the target but not the close-coupling expansion [12], that are included in our version of STG3, and not in the QUB version. They have been implemented in the parallel version.

In an ICFT calculation, we generate the unphysical K-matrices in LS coupling using a version of Seaton's unpublished program STGF, that has been modified by Badnell *et al* [13] to incorporate MQDT as an option. Finally, we employ our STGICF program to transform the unphysical K-matrices to intermediate coupling, generate the physical K-matrices and then calculate the collision strengths. These outer-region codes have now both been modified to operate on distributed-memory parallel computers.

Typically $\approx 10^4$ energy points are required in order to resolve the many resonances in a large calculation. Since every calculation is independent, data parallelization is an effective way to treat these large-scale problems. The energy points, at which the collision strengths are to be evaluated, are distributed among the number of available processors. The computational time required for a given energy is strongly affected by the number of open channels. Therefore, care must be taken in order to ensure that the more time-consuming energy regions are equally partitioned among all of the processors. For cases in which the number of energy points is much larger than the number of processors, this is easy to implement. We normally calculate the collision strengths at N energy points using a constant mesh separation ΔE. We distribute the calculation over M processors $p = 0, \ldots, M-1$, in such a way that every processor calculates roughly $N_p = N/M$ points. The balance is achieved by having processor p calculate the collision strengths at points $E_k = E_0 + (k \times M + p)\Delta E$, $k = 0, \ldots, N_p - 1$, where E_0 is the initial mesh point. If the mesh separation ΔE is small, the number of open channels at any step k remains approximately the same for every processor. This approach has the additional advantage of reducing the memory requirements for storing the K-matrices. The matrices are kept in (fast access) memory rather than stored in (slow access) disk files.

Scalability of STG3, STGF and STGICF has been achieved, at least with the use of 64 processors. For the 180-level calculation on Ne^{5+}, STG3 required 55 h of total CPU time on the Cray T3E-900 Supercomputer at the National Energy Research Scientific Computing Center (NERSC) in Oakland, CA. The asymptotic codes were run on the IBM SP Supercomputer at NERSC. For 11 648 energy mesh points, STGF required 206 h of total CPU time, while STGICF consumed a total of 410 h. Thus STG3, STGF and STGICF required almost 28 days of total CPU time. However, this entire calculation ran in half a day using 64 processors.

3. Description of the calculations

3.1. Target-state calculations

The bound-state radial wavefunctions employed in our scattering calculations were generated using Froese Fischer's multi-configuration Hartree–Fock (MCHF) programs [14]. The 1s, 2s

and 2p, orbitals were determined from a Hartree–Fock (HF) calculation on the $2s^2 2p$ ground configuration, while the 3ℓ and 4ℓ orbitals were generated from frozen-core HF calculations on the $2s^2 n\ell$ configurations. We also included three pseudo-orbitals in order to partially correct the spectroscopic orbitals for variations between configurations. A $\overline{5}$p pseudo-orbital was generated from an MCHF calculation in which the energy of the $2p^3\ {}^2P$ term was minimized and in which the $2p^3\ {}^2P$, $2p^2 3p\ {}^2P$, $2p^2 4p\ {}^2P$, and $2p^2\overline{5}p\ {}^2P$ terms were included. $\overline{5}$s and $\overline{5}$d pseudo-orbitals were determined from an MCHF calculation in which the energy of the $2s2p^2\ {}^2P$ term was minimized and in which the $2s2p^2\ {}^2P$, $2p^2 3s\ {}^2P$, $2p^2 3d\ {}^2P$, $2p^2 4s\ {}^2P$, $2p^2 4d\ {}^2P$ $2p^2\overline{5}s\ {}^2P$ and $2p^2\overline{5}d\ {}^2P$ terms were included.

This set of orbitals was then employed in a large Breit–Pauli CI calculation. It included the odd-parity levels arising from the $2s^2 2p$, $2p^3$, $2s^2 3p$, 2s2p3s, 2s2p3d, $2s^2 4p$, $2s^2 4f$, $2p^2 3p$, 2s2p4s, 2s2p4d, $2p^2 4p$, $2p^2\overline{5}p$, $2s2p\overline{5}s$ and $2s2p\overline{5}d$ configurations; the even-parity levels included were those arising from the configurations $2s2p^2$, $2s^2 3s$, $2s^2 3d$, 2s2p3p, $2s^2 4s$, $2s^2 4d$, $2p^2 3s$, $2p^2 3d$, 2s2p4p, $2p^2 4s$, $2p^2 4d$, $2p^2\overline{5}s$, $2p^2\overline{5}d$ and $2s2p\overline{5}p$.

3.2. Scattering calculations

Here we describe our scattering calculations for the electron-impact excitation of Ne^{5+} using the intermediate-coupling frame-transformation R-matrix method. We first performed an 11-term, 20-level ICFT calculation in which we employed the large CI expansion discussed above to describe the target. Here the close-coupling expansion in LS coupling included the 11 terms arising from the $2s^2 2p$, $2s2p^2$, $2p^3$ and $2s^2 3\ell$ configurations. The size of the R-matrix box was 11.5 au, we used 25 basis orbitals to represent the continuum for each value of the angular momentum and all $LS\Pi$ partial waves from $L = 0$ to 14 were included. We generated unphysical K-matrices in LS coupling and then employed the ICFT method to transform the unphysical K-matrices to intermediate coupling; finally, we determined the physical K-matrices in intermediate coupling for all $J\Pi$ partial waves from $J = 0$ to 12. In order to improve on the accuracy of the scattering calculations, the theoretical target energies were adjusted to the experimental values.

For the 20-level results reported here, we employed an energy mesh in the resonance region with a mesh spacing of 1.0×10^{-3} Ry; above all thresholds, we employed a mesh spacing of 6.6×10^{-2} Ry up to an energy of 24 Ry, for a total of 7674 mesh points. We performed several tests to ensure that this energy mesh was sufficiently fine so as to resolve the dominant resonance contributions; this will be discussed further in our description of the determination of effective collision strengths.

A $J\Pi$ partial-wave expansion up to $J = 12$, is not sufficiently complete for the determination of collision strengths up to an energy of 24 Ry. Thus, we performed an R-matrix calculation without exchange for all $LS\Pi$ partial waves from $L = 11$ to 42 and then used the ICFT method to generate physical K-matrices in intermediate coupling for all $J\Pi$ partial waves from $J = 13$ to 40. These high-J contributions were then topped-up as follows: the dipole-allowed transitions were topped-up using a method originally described by Burgess [15] for LS coupling and implemented here for intermediate coupling; the non-dipole transitions were topped-up assuming a geometric series in J, using energy ratios, and with a special procedure for handling transitions between nearly degenerate levels based on the degenerate limiting case [16]. Finally, it is important to note that in the asymptotic region, we included the long-range multipole potentials perturbatively for all partial waves.

For our 180-level ICFT R-matrix calculation, we first performed an R-matrix calculation with exchange in LS coupling for which the close-coupling expansion included all 83 terms of the $2s^2 2p$, $2s2p^2$, $2p^3$, $2s^2 3\ell$, $2s^2 4\ell$, $2s2p3\ell$, $2p^2 3\ell$, 2s2p4s, 2s2p4p and 2s2p4d configurations.

We employed the same CI expansion of the target as we employed in the 20-level calculation. Therefore, the details regarding the 180-level ICFT calculation, including the no-exchange part of the calculation and top-up, are identical to those given above. Again the theoretical target energies were adjusted to the experimental values; however, there were no experimental energies available for a number of the 180 levels included here, and some of the experimental fine-structure levels arising from a given term are degenerate. Thus we had to make some adjustments in order to obtain a consistent set of target energies for this calculation. First we used the experimental values for the average energy of the degenerate fine-structure energies, but adjusted the energy spacing to the theoretical values of the fine-structure splitting. Secondly, where possible, we adjusted the theoretical energies for levels for which there were no experimental values according to the average difference between experiment and theory for known levels arising from the same configuration and the same parent. Of course, for levels where no experimental values were available and no such adjustments were possible, the theoretical energies were employed.

For the 180-level calculations we used an energy mesh similar to that employed for the 20-level calculation; however, for technical reasons associated with the number of processors employed, they were slightly different. In the resonance region the mesh-spacing was 9.9×10^{-4} Ry, while above all thresholds it was equal to 9.9×10^{-2} Ry up to the maximum energy of 24 Ry, for a total of 11 648 mesh points. Again we performed tests on this energy mesh to be sure that it resolved the dominant resonance contributions.

3.3. Determination of effective collision strengths

The effective collision strength, Υ, first introduced by Seaton [17], is defined by the equation

$$\Upsilon_{ij} = \int_0^\infty \Omega(i \rightarrow j) \exp\left(\frac{-\epsilon_j}{kT_e}\right) \mathrm{d}\left(\frac{\epsilon_j}{kT_e}\right), \tag{1}$$

where Ω is the collision strength for the transition from level i to level j and ϵ_j is the continuum energy of the final scattered electron. We employed the integration technique of Burgess and Tully [18] to calculate the effective collision strengths. One must use some approximate technique for that part of the integration in equation (1) above the highest energy for which the collision strengths have been calculated. We employ an interpolation method to the infinite-energy limit for the collision strengths as discussed in detail in Whiteford *et al* [19]. In order to test the accuracy of these interpolations, we recorded a number of plots of the reduced collision strengths as a function of reduced energy, as described by Burgess and Tully [18]. We found that all plots for transitions among the $n = 2$ levels went smoothly to their infinite-energy limits. However, for transitions to the higher lying levels, some of these curves made more abrupt changes in slope in the region where the interpolations began. For this reason, we limited our calculations of effective collision strengths to temperatures of up to 2.5×10^6 K, so that any errors in these interpolations will have a very minor effect on the effective collision strengths.

We used the calculated effective collision strengths to test the ability of our energy mesh to resolve narrow resonances. Because the 20-level calculation was relatively fast, even on a single processor, we actually employed two energy meshes. The first one, described above, used a spacing of 1.0×10^{-3} Ry in the resonance region; for the second mesh, we employed a spacing of 2.5×10^{-4} Ry. We then compared the calculated effective collision strengths. We found that they were very close for the majority of transitions and differed by more than 10% in only a small number of the weaker transitions. For the mesh with a spacing of 1.0×10^{-3} Ry, we then eliminated all resonances for which the resonance peak occurred at a single mesh point and was more than a factor of ten greater than the background

collision strength at the two adjacent mesh points. We compared collision strengths calculated without the elimination of unresolved resonances with those calculated after the removal of such resonances. Again the differences were negligible for the vast majority of transitions, and differences of more than 10% occurred in only a small number of the weaker transitions. These results indicate that the mesh spacing of 1.0×10^{-3} Ry was sufficiently fine for the 20-level calculation.

Even on a massively parallel machine, it would have been prohibitively expensive to employ a mesh spacing of 2.5×10^{-4} Ry for the 180-level calculation. Thus we used a mesh spacing of 9.9×10^{-4} Ry in the resonance region. We then compared the effective collision strengths with and without the elimination of unresolved resonances, as described above. The comparisons were quite similar, with differences of more than 10% occurring for a small fraction of the weaker transitions. The final results, presented here, employed the collision strengths with the elimination of resonances that occurred at a single mesh point and had a peak height of more than a factor of ten greater than the background collision strengths. We believe that this should provide the most accurate overall results.

4. Results

4.1. Bound-state energies and radiative rates

The energies determined from our Breit–Pauli CI calculations of the Ne^{5+} target are presented in table 1. They are arranged in the order of the theoretical energies; however, the order of the energies employed in the *R*-matrix calculations as described in the last section are listed in the last column of this table. For the most part, the agreement between the experimental and theoretical energies is quite good; the largest deviation is 4.4% for the $2s2p^2(^1S)^2S_{1/2}$ level, while the deviations for the vast majority of the other levels are much smaller.

In table 2, we present our calculated radiative rates for all possible dipole-allowed transitions among the lowest 20 levels for which the radiative rates are greater than 10^4 s^{-1}. These are compared to the radiative rates available from the MCHF/MCDF Collection on the Internet[4]. The overall agreement between these two sets of data is good; the average difference for all transitions given in the table is 24%. The level of agreement is further illustrated in figure 1, where we show a graphical comparison of the present radiative rates with those from the MCHF/MCDF Collection. We see that most of the rates for the stronger transitions agree very well; in fact, for rates above 10^8 s^{-1} the average difference is only 6%. As one can see from figure 1, the deviations between these two sets of data are much larger for the transitions with radiative rates between 10^4 and 10^8 s^{-1}—the average difference between these two sets of radiative rates for these weaker transitions is 49%. However, this should be expected since these rates are extremely sensitive to weak mixing between states; in fact, it is somewhat surprising that the agreement is as good as it is for a number of these weak transitions.

All the radiative rates presented in table 2 and figure 1 were calculated in the length gauge. We have compared our calculated rates given in table 2 with those calculated in the velocity gauge and found an average difference of 46%. However, as one would expect, the vast majority of the larger differences between these two forms is concentrated in the very weakest transitions. There is an average difference of 87% for the 30 transitions in table 2 with rates below 10^8 s^{-1}, while the average difference between these two forms for the 41 transitions with rates above 10^8 s^{-1} is 16%.

[4] http:/www.vuse.vanderbilt.edu/∼georgio/html_doc/header.html.

Table 1. Energies in Rydbergs for the levels included in the 180-level ICFT *R*-matrix calculation for Ne^{5+} relative to the $2s^2 2p\ ^2P_{1/2}$ ground level. No experimental values exist for the numbers in (); they were estimated from the average difference between theory and experiment for levels of the same configuration and with the same parent. The experimental levels in {} are degenerate and were adjusted to have the theoretical fine structure splittings. The column labelled 'order', indicates the order of levels employed in the *R*-matrix calculation.

Level no	Level	Energy (Th.)	Energy (Exp.[a])	Diff.	Order
1	$2s^2 2p\ ^2P_{1/2}$	0.0000	0.0000	0.0000	1
2	$2s^2 2p\ ^2P_{3/2}$	0.0118	0.0119	−0.0001	2
3	$2s2p^2(^3P)\ ^4P_{1/2}$	0.9078	0.9137	−0.0059	3
4	$2s2p^2(^3P)\ ^4P_{3/2}$	0.9119	0.9177	−0.0058	4
5	$2s2p^2(^3P)\ ^4P_{5/2}$	0.9187	0.9235	−0.0048	5
6	$2s2p^2(^1D)\ ^2D_{3/2}$	1.6799	1.6314	0.0485	7
7	$2s2p^2(^1D)\ ^2D_{5/2}$	1.6800	1.6311	0.0489	6
8	$2s2p^2(^1S)\ ^2S_{1/2}$	2.1959	2.1037	0.0922	8
9	$2s2p^2(^3P)\ ^2P_{1/2}$	2.3140	2.2717	0.0423	9
10	$2s2p^2(^3P)\ ^2P_{3/2}$	2.3217	2.2792	0.0425	10
11	$2p^3\ ^4S_{3/2}$	2.9706	2.9304	0.0402	11
12	$2p^3\ ^2D_{3/2}$	3.3347	{3.2754}	{0.0593}	12
13	$2p^3\ ^2D_{5/2}$	3.3350	{3.2757}	{0.0593}	13
14	$2p^3\ ^2P_{1/2}$	3.8054	3.6996	0.1008	14
15	$2p^3\ ^2P_{3/2}$	3.8063	3.7003	0.1060	15
16	$2s^2 3s\ ^2S_{1/2}$	6.5970	6.5849	0.0121	16
17	$2s^2 3p\ ^2P_{1/2}$	7.0448	7.0280	0.0168	17
18	$2s^2 3p\ ^2P_{3/2}$	7.0473	7.0309	0.0164	18
19	$2s^2 3d\ ^2D_{3/2}$	7.4807	{7.4387}	{0.0420}	19
20	$2s^2 3d\ ^2D_{5/2}$	7.4815	{7.4395}	{0.0420}	20
21	$2s2p(^3P)3s\ ^4P_{1/2}$	7.6106	7.5961	0.0145	21
22	$2s2p(^3P)3s\ ^4P_{3/2}$	7.6146	7.6004	0.0142	22
23	$2s2p(^3P)3s\ ^4P_{5/2}$	7.6214	7.6074	0.0140	23
24	$2s2p(^3P)3s\ ^2P_{1/2}$	7.8420	7.7981	0.0439	24
25	$2s2p(^3P)3s\ ^2P_{3/2}$	7.8495	7.8056	0.0439	25
26	$2s2p(^3P)3p\ ^2P_{1/2}$	7.9990	7.9844	0.0146	26
27	$2s2p(^3P)3p\ ^2P_{3/2}$	8.0025	7.9887	0.0138	27
28	$2s2p(^3P)3p\ ^4D_{1/2}$	8.0179	(7.9920)	—	28
29	$2s2p(^3P)3p\ ^4D_{3/2}$	8.0201	(7.9942)	—	29
30	$2s2p(^3P)3p\ ^4D_{5/2}$	8.0240	8.0057	0.0183	30
31	$2s2p(^3P)3p\ ^4D_{7/2}$	8.0300	8.0117	0.0183	31
32	$2s2p(^3P)3p\ ^4S_{3/2}$	8.1061	(8.0802)	—	32
33	$2s2p(^3P)3p\ ^4P_{1/2}$	8.1800	(8.1541)	—	33
34	$2s2p(^3P)3p\ ^4P_{3/2}$	8.1827	(8.1568)	—	34
35	$2s2p(^3P)3p\ ^4P_{5/2}$	8.1866	(8.1607)	—	35
36	$2s2p(^3P)3p\ ^2D_{3/2}$	8.2418	8.2023	0.0395	36
37	$2s2p(^3P)3p\ ^2D_{5/2}$	8.2490	8.2096	0.0394	37
38	$2s2p(^3P)3d\ ^4F_{3/2}$	8.3809	(8.3333)	—	38
39	$2s2p(^3P)3p\ ^2S_{1/2}$	8.3828	8.3368	0.0460	40
40	$2s2p(^3P)3d\ ^4F_{5/2}$	8.3834	(8.3358)	—	39
41	$2s2p(^3P)3d\ ^4F_{7/2}$	8.3868	(8.3392)	—	41
42	$2s2p(^3P)3d\ ^4F_{9/2}$	8.3914	(8.3438)	—	42
43	$2s2p(^3P)3d\ ^4D_{1/2}$	8.4739	8.4408	0.0331	43
44	$2s2p(^3P)3d\ ^4D_{3/2}$	8.4746	8.4417	0.0329	44
45	$2s2p(^3P)3d\ ^4D_{5/2}$	8.4759	8.4426	0.0333	45
46	$2s2p(^3P)3d\ ^4D_{7/2}$	8.4782	8.4454	0.0328	46
47	$2s2p(^3P)3d\ ^2D_{3/2}$	8.5025	8.4567	0.0458	47

Table 1. (Continued.)

Level no	Level	Energy (Th.)	Energy (Exp.[a])	Diff.	Order
48	$2s2p(^3P)3d\ ^2D_{5/2}$	8.5037	8.4586	0.0451	48
49	$2s2p(^3P)3d\ ^4P_{5/2}$	8.5188	8.4894	0.0294	49
50	$2s2p(^3P)3d\ ^4P_{3/2}$	8.5212	8.4921	0.0291	50
51	$2s2p(^3P)3d\ ^4P_{1/2}$	8.5227	8.4944	0.0283	51
52	$2s2p(^1P)3s\ ^2P_{3/2}$	8.6617	{8.5681}	{0.0936}	52
53	$2s2p(^1P)3s\ ^2P_{1/2}$	8.6622	{8.5686}	{0.0936}	53
54	$2s2p(^3P)3d\ ^2F_{5/2}$	8.6897	8.6197	0.0700	54
55	$2s2p(^3P)3d\ ^2F_{7/2}$	8.6967	8.6270	0.0697	55
56	$2s2p(^3P)3d\ ^2P_{3/2}$	8.7437	8.6771	0.0666	56
57	$2s2p(^3P)3d\ ^2P_{1/2}$	8.7467	8.6808	0.0659	57
58	$2s^24s\ ^2S_{1/2}$	8.9415	8.9578	−0.0163	58
59	$2s2p(^1P)3p\ ^2D_{3/2}$	9.0958	8.9851	0.1107	59
60	$2s2p(^1P)3p\ ^2D_{5/2}$	9.0970	8.9864	0.1106	60
61	$2s2p(^1P)3p\ ^2P_{1/2}$	9.0972	9.0001	0.0971	61
62	$2s2p(^1P)3p\ ^2P_{3/2}$	9.0997	9.0029	0.0968	62
63	$2s^24p\ ^2P_{1/2}$	9.1628	—	—	64
64	$2s^24p\ ^2P_{3/2}$	9.1639	—	—	65
65	$2s2p(^1P)3p\ ^2S_{1/2}$	9.2495	9.0580	0.1912	63
66	$2s^24d\ ^2D_{3/2}$	9.3194	{9.2861}	{0.0333}	66
67	$2s^24d\ ^2D_{5/2}$	9.3197	{9.2864}	{0.0333}	67
68	$2p^2(^3P)3s\ ^4P_{1/2}$	9.3432	{9.3177}	{0.0255}	70
69	$2p^2(^3P)3s\ ^4P_{3/2}$	9.3473	{9.3218}	{0.0255}	71
70	$2p^2(^3P)3s\ ^4P_{5/2}$	9.3540	{9.3285}	{0.0255}	72
71	$2s2p(^1P)3d\ ^2F_{5/2}$	9.3858	{9.3132}	{0.0726}	68
72	$2s2p(^1P)3d\ ^2F_{7/2}$	9.3859	{9.3133}	{0.0726}	69
73	$2s2p(^1P)3d\ ^2D_{3/2}$	9.5176	9.3871	0.1305	73
74	$2s2p(^1P)3d\ ^2D_{5/2}$	9.5187	9.3882	0.1305	74
75	$2p^2(^3P)3s\ ^2P_{1/2}$	9.5461	—	—	77
76	$2p^2(^3P)3s\ ^2P_{3/2}$	9.5536	—	—	78
77	$2p^2(^3P)3p\ ^2S_{1/2}$	9.6137	—	—	79
78	$2s2p(^1P)3d\ ^2P_{1/2}$	9.6222	{9.4068}	{0.2152}	75
79	$2s2p(^1P)3d\ ^2P_{3/2}$	9.6232	{9.4075}	{0.2152}	76
80	$2s^24f\ ^2F_{5/2}$	9.6864	—	—	86
81	$2s^24f\ ^2F_{7/2}$	9.6865	—	—	87
82	$2p^2(^3P)3p\ ^4D_{1/2}$	9.6905	{9.6706}	{0.0199}	82
83	$2p^2(^3P)3p\ ^4D_{3/2}$	9.6930	{9.6731}	{0.0199}	83
84	$2p^2(^3P)3p\ ^4D_{5/2}$	9.6972	{9.6773}	{0.0199}	84
85	$2p^2(^3P)3p\ ^4D_{7/2}$	9.7032	{9.6833}	{0.0199}	85
86	$2p^2(^1D)3s\ ^2D_{3/2}$	9.7313	{9.6248}	{0.1065}	80
87	$2p^2(^1D)3s\ ^2D_{5/2}$	9.7317	{9.6252}	{0.1065}	81
88	$2p^2(^3P)3p\ ^4P_{1/2}$	9.7367	9.7068	0.0299	88
89	$2p^2(^3P)3p\ ^4P_{3/2}$	9.7391	9.7102	0.0289	89
90	$2p^2(^3P)3p\ ^4P_{5/2}$	9.7433	9.7154	0.0279	90
91	$2p^2(^3P)3p\ ^2D_{3/2}$	9.8091	(9.7872)	—	91
92	$2p^2(^3P)3p\ ^2D_{5/2}$	9.8167	(9.7948)	—	92
93	$2p^2(^3P)3p\ ^2P_{1/2}$	9.8874	(9.8655)	—	93
94	$2p^2(^3P)3p\ ^2P_{3/2}$	9.8888	(9.8669)	—	94
95	$2p^2(^3P)3p\ ^4S_{3/2}$	9.9086	9.8969	0.0117	95
96	$2s2p(^3P)4s\ ^4P_{1/2}$	10.0189	—	—	98
97	$2p^2(^3P)3d\ ^4F_{3/2}$	10.0200	—	—	99

Table 1. (Continued.)

Level no	Level	Energy (Th.)	Energy (Exp.[a])	Diff.	Order
98	$2p^2(^3P)3d\ ^4F_{5/2}$	10.0224	—	—	100
99	$2s2p(^3P)4s\ ^4P_{3/2}$	10.0229	—	—	101
100	$2p^2(^3P)3d\ ^4F_{7/2}$	10.0258	—	—	102
101	$2s2p(^3P)4s\ ^4P_{5/2}$	10.0296	—	—	103
102	$2p^2(^3P)3d\ ^4F_{9/2}$	10.0303	—	—	104
103	$2p^2(^3P)3d\ ^4D_{1/2}$	10.0744	—	—	105
104	$2p^2(^3P)3d\ ^4D_{3/2}$	10.0758	—	—	106
105	$2p^2(^3P)3d\ ^4D_{5/2}$	10.0781	—	—	107
106	$2p^2(^3P)3d\ ^4D_{7/2}$	10.0807	—	—	108
107	$2p^2(^3P)3d\ ^2P_{3/2}$	10.0845	—	—	109
108	$2s2p(^3P)4s\ ^2P_{1/2}$	10.0871	—	—	110
109	$2p^2(^3P)3d\ ^2P_{1/2}$	10.0900	—	—	111
110	$2s2p(^3P)4s\ ^2P_{3/2}$	10.0931	—	—	112
111	$2p^2(^1D)3p\ ^2F_{5/2}$	10.0984	9.9859	0.1126	96
112	$2p^2(^1D)3p\ ^2F_{7/2}$	10.1004	9.9890	0.1114	97
113	$2p^2(^3P)3d\ ^2F_{5/2}$	10.1527	—	—	115
114	$2p^2(^3P)3d\ ^2F_{7/2}$	10.1608	—	—	116
115	$2p^2(^3P)3d\ ^4P_{5/2}$	10.1628	—	—	117
116	$2p^2(^3P)3d\ ^4P_{3/2}$	10.1636	—	—	118
117	$2p^2(^3P)3d\ ^4P_{1/2}$	10.1640	—	—	119
118	$2s2p(^3P)4p\ ^4D_{1/2}$	10.1928	—	—	120
119	$2s2p(^3P)4p\ ^4D_{3/2}$	10.1949	—	—	121
120	$2p^2(^1D)3p\ ^2D_{5/2}$	10.1963	{10.0999}	{0.0964}	113
121	$2p^2(^1D)3p\ ^2D_{3/2}$	10.1970	{10.1006}	{0.0964}	114
122	$2s2p(^3P)4p\ ^4D_{5/2}$	10.1983	—	—	122
123	$2s2p(^3P)4p\ ^4S_{3/2}$	10.2009	—	—	123
124	$2s2p(^3P)4p\ ^4D_{7/2}$	10.2032	—	—	124
125	$2s2p(^3P)4p\ ^2P_{1/2}$	10.2113	—	—	125
126	$2s2p(^3P)4p\ ^2P_{3/2}$	10.2138	—	—	126
127	$2s2p(^3P)4p\ ^2D_{3/2}$	10.2394	{10.2361}	{0.0033}	129
128	$2s2p(^3P)4p\ ^4P_{1/2}$	10.2444	—	—	131
129	$2s2p(^3P)4p\ ^2D_{5/2}$	10.2449	{10.2416}	{0.0033}	130
130	$2s2p(^3P)4p\ ^4P_{3/2}$	10.2457	—	—	132
131	$2s2p(^3P)4p\ ^4P_{5/2}$	10.2476	—	—	133
132	$2s2p(^3P)4p\ ^2S_{1/2}$	10.2917	—	—	140
133	$2s2p(^3P)4d\ ^4F_{3/2}$	10.2998	(10.2599)	—	134
134	$2s2p(^3P)4d\ ^4F_{5/2}$	10.3020	(10.2621)	—	135
135	$2s2p(^3P)4d\ ^4F_{7/2}$	10.3053	(10.2654)	—	136
136	$2s2p(^3P)4d\ ^4F_{9/2}$	10.3099	(10.2700)	—	137
137	$2p^2(^1D)3p\ ^2P_{1/2}$	10.3204	(10.2150)	—	127
138	$2p^2(^1D)3p\ ^2P_{3/2}$	10.3245	(10.2191)	—	128
139	$2s2p(^3P)4d\ ^4D_{1/2}$	10.3360	10.3028	0.0332	141
140	$2s2p(^3P)4d\ ^4D_{3/2}$	10.3362	10.3032	0.0330	142
141	$2s2p(^3P)4d\ ^4D_{5/2}$	10.3369	10.3055	0.0314	143
142	$2s2p(^3P)4d\ ^4D_{7/2}$	10.3402	10.3073	0.0329	144
143	$2s2p(^3P)4d\ ^4P_{5/2}$	10.3491	10.3210	0.0281	147
144	$2s2p(^3P)4d\ ^4P_{3/2}$	10.3518	10.3219	0.0299	148
145	$2s2p(^3P)4d\ ^2D_{3/2}$	10.3534	{10.3155}	{0.0379}	145
146	$2s2p(^3P)4d\ ^4P_{1/2}$	10.3536	10.3228	0.0308	149
147	$2s2p(^3P)4d\ ^2D_{5/2}$	10.3556	{10.3177}	{0.0379}	146

Table 1. (Continued.)

Level no	Level	Energy (Th.)	Energy (Exp.[a])	Diff.	Order
148	$2p^2(^3P)3d\ ^2D_{3/2}$	10.3924	—	—	156
149	$2p^2(^3P)3d\ ^2D_{5/2}$	10.3941	—	—	157
150	$2p^2(^1S)3s\ ^2S_{1/2}$	10.4056	—	—	160
151	$2s2p(^3P)4d\ ^2F_{5/2}$	10.4208	10.3717	0.0491	152
152	$2p^2(^1D)3d\ ^2G_{7/2}$	10.4251	(10.2764)	—	138
153	$2p^2(^1D)3d\ ^2G_{9/2}$	10.4259	(10.2775)	—	139
154	$2s2p(^3P)4d\ ^2F_{7/2}$	10.4271	10.3790	0.0481	153
155	$2s2p(^3P)4d\ ^2P_{3/2}$	10.4352	(10.3953)	—	158
156	$2s2p(^3P)4d\ ^2P_{1/2}$	10.4391	(10.3992)	—	159
157	$2p^2(^1D)3d\ ^2D_{3/2}$	10.5033	(10.3549)	—	150
158	$2p^2(^1D)3d\ ^2D_{5/2}$	10.5035	(10.3551)	—	151
159	$2p^2(^1D)3d\ ^2F_{7/2}$	10.5043	{10.3833}	{0.1210}	154
160	$2p^2(^1D)3d\ ^2F_{5/2}$	10.5083	{10.3873}	{0.1210}	155
161	$2p^2(^1D)3d\ ^2P_{1/2}$	10.6208	10.4085	0.2123	161
162	$2p^2(^1D)3d\ ^2P_{3/2}$	10.6233	10.4112	0.2121	162
163	$2p^2(^1D)3d\ ^2S_{1/2}$	10.6831	(10.5347)	—	163
164	$2p^2(^1S)3p\ ^2P_{1/2}$	10.8195	—	—	164
165	$2p^2(^1S)3p\ ^2P_{3/2}$	10.8208	—	—	165
166	$2s2p(^1P)4s\ ^2P_{1/2}$	11.0673	—	—	166
167	$2s2p(^1P)4s\ ^2P_{3/2}$	11.0679	—	—	167
168	$2p^2(^1S)3d\ ^2D_{5/2}$	11.1422	—	—	168
169	$2p^2(^1S)3d\ ^2D_{3/2}$	11.1427	—	—	169
170	$2s2p(^1P)4p\ ^2P_{1/2}$	11.2281	—	—	170
171	$2s2p(^1P)4p\ ^2P_{3/2}$	11.2289	—	—	171
172	$2s2p(^1P)4p\ ^2D_{3/2}$	11.2467	—	—	172
173	$2s2p(^1P)4p\ ^2D_{5/2}$	11.2469	—	—	173
174	$2s2p(^1P)4p\ ^2S_{1/2}$	11.2661	—	—	174
175	$2s2p(^1P)4d\ ^2F_{7/2}$	11.3547	—	—	175
176	$2s2p(^1P)4d\ ^2F_{5/2}$	11.3548	—	—	176
177	$2s2p(^1P)4d\ ^2D_{3/2}$	11.3629	—	—	177
178	$2s2p(^1P)4d\ ^2D_{5/2}$	11.3633	—	—	178
179	$2s2p(^1P)4d\ ^2P_{1/2}$	11.4002	—	—	179
180	$2s2p(^1P)4d\ ^2P_{3/2}$	11.4005	—	—	180

[a] Kelly [20].

4.2. Collision strengths and effective collision strengths

In this section, we provide only a small representative sample of our excitation data among the lowest seven levels of Ne^{5+}. In figure 2, we compare the collision strength determined from the 20-level calculation with that from the 180-level calculation for the important fine-structure transition $2s^22p\ ^2P_{1/2} \rightarrow 2s^22p\ ^2P_{3/2}$. As we can see, the two calculated collision strengths are very similar, both in terms of the background and the resonance contributions. Thus the effects of coupling to the higher levels included in only the 180-level calculation, as well as resonance contributions from these higher levels, are small for this transition.

The collision strengths for the transitions from both the $2s^22p\ ^2P_{1/2}$ ground level and the $2s^22p\ ^2P_{3/2}$ excited level to the $2s2p^2(^3P)\ ^4P_{3/2}$ level are shown in figure 3. These transitions are only weakly dipole-allowed through the spin–orbit interaction. In this figure, we see the added resonance contributions in both transitions arising from the higher levels included in

Table 2. Electric-dipole radiative rates for all possible transitions among the lowest 20 levels in Ne^{5+} with rates greater than 10^4 s^{-1}. The level numbers for each ($j \rightarrow i$) transition given in the first two columns of this table are the those listed in the last column of table 1.

j	i	Transition	Present[a]	MCHF/MCDF Collection[b]
3	1	$2s2p^2\ ^4P_{1/2}$–$2s^22p\ ^2P_{1/2}$	1.18×10^4	1.38×10^4
7	1	$2s2p^2\ ^2D_{3/2}$–$2s^22p\ ^2P_{1/2}$	1.02×10^9	9.88×10^8
8	1	$2s2p^2\ ^2S_{1/2}$–$2s^22p\ ^2P_{1/2}$	2.13×10^9	2.03×10^9
9	1	$2s2p^2\ ^2P_{1/2}$–$2s^22p\ ^2P_{1/2}$	6.54×10^9	6.66×10^9
10	11	$2s2p^2\ ^2P_{3/2}$–$2s^22p\ ^2P_{1/2}$	1.73×10^9	1.73×10^9
16	1	$2s^23s\ ^2S_{1/2}$–$2s^22p\ ^2P_{1/2}$	9.33×10^9	9.91×10^9
19	1	$2s^23d\ ^2D_{3/2}$–$2s^22p\ ^2P_{1/2}$	1.26×10^{11}	1.26×10^{11}
3	2	$2s2p^2\ ^4P_{1/2}$–$2s^22p\ ^2P_{3/2}$	1.06×10^4	1.25×10^4
6	2	$2s2p^2\ ^2D_{5/2}$–$2s^22p\ ^2P_{3/2}$	1.17×10^9	1.14×10^9
7	2	$2s2p^2\ ^2D_{3/2}$–$2s^22p\ ^2P_{3/2}$	1.84×10^8	1.78×10^8
8	2	$2s2p^2\ ^2S_{1/2}$–$2s^22p\ ^2P_{3/2}$	3.17×10^9	3.27×10^9
9	2	$2s2p^2\ ^2P_{1/2}$–$2s^22p\ ^2P_{3/2}$	3.85×10^9	3.74×10^9
10	2	$2s2p^2\ ^2P_{3/2}$–$2s^22p\ ^2P_{3/2}$	8.70×10^9	8.70×10^9
16	2	$2s^23s\ ^2S_{1/2}$–$2s^22p\ ^2P_{3/2}$	1.88×10^9	1.99×10^9
19	2	$2s^23d\ ^2D_{3/2}$–$2s^22p\ ^2P_{3/2}$	2.52×10^{10}	2.52×10^{10}
20	2	$2s^23d\ ^2D_{5/2}$–$2s^22p\ ^2P_{3/2}$	1.51×10^{11}	1.51×10^{11}
11	3	$2p^3\ ^4S_{3/2}$–$2s2p^2\ ^4P_{1/2}$	1.57×10^9	1.57×10^9
14	3	$2p^3\ ^2P_{1/2}$–$2s2p^2\ ^4P_{1/2}$	1.08×10^5	1.37×10^5
17	3	$2s^23p\ ^2P_{1/2}$–$2s2p^2\ ^4P_{1/2}$	3.67×10^4	4.07×10^4
11	4	$2p^3\ ^4S_{3/2}$–$2s2p^2\ ^4P_{3/2}$	3.13×10^9	3.11×10^9
12	4	$2p^3\ ^2D_{3/2}$–$2s2p^2\ ^4P_{3/2}$	1.10×10^5	1.41×10^5
13	4	$2p^3\ ^2D_{5/2}$–$2s2p^2\ ^4P_{3/2}$	1.16×10^4	1.15×10^4
14	4	$2p^3\ ^2P_{1/2}$–$2s2p^2\ ^4P_{3/2}$	2.15×10^4	2.86×10^4
15	4	$2p^3\ ^2P_{3/2}$–$2s2p^2\ ^4P_{3/2}$	2.44×10^5	3.34×10^5
17	4	$2s^23p\ ^2P_{1/2}$–$2s2p^2\ ^4P_{3/2}$	9.31×10^4	6.73×10^4
11	5	$2p^3\ ^4S_{3/2}$–$2s2p^2\ ^4P_{5/2}$	4.65×10^9	4.63×10^9
12	5	$2p^3\ ^2D_{3/2}$–$2s2p^2\ ^4P_{5/2}$	3.03×10^4	2.55×10^4
13	5	$2p^3\ ^2D_{5/2}$–$2s2p^2\ ^4P_{5/2}$	3.62×10^5	4.52×10^5
15	5	$2p^3\ ^2P_{3/2}$–$2s2p^2\ ^4P_{5/2}$	3.10×10^5	2.60×10^5
18	5	$2s^23p\ ^2P_{3/2}$–$2s2p^2\ ^4P_{5/2}$	1.04×10^5	1.12×10^5
12	6	$2p^3\ ^2D_{3/2}$–$2s2p^2\ ^2D_{5/2}$	2.63×10^8	2.68×10^8
13	6	$2p^3\ ^2D_{3/2}$–$2s2p^2\ ^2D_{5/2}$	2.21×10^9	2.32×10^9
15	6	$2p^3\ ^2P_{3/2}$–$2s2p^2\ ^2D_{5/2}$	3.85×10^9	3.76×10^9
18	6	$2s^23p\ ^2P_{3/2}$–$2s2p^2\ ^2D_{5/2}$	2.82×10^9	1.90×10^9
12	7	$2p^3\ ^2D_{3/2}$–$2s2p^2\ ^2D_{3/2}$	2.09×10^9	2.11×10^9
13	7	$2p^3\ ^2D_{5/2}$–$2s2p^2\ ^2D_{3/2}$	1.68×10^8	1.69×10^8
14	7	$2p^3\ ^2P_{1/2}$–$2s2p^2\ ^2D_{3/2}$	4.37×10^9	4.29×10^9
15	7	$2p^3\ ^2P_{3/2}$–$2s2p^2\ ^2D_{3/2}$	4.58×10^8	4.54×10^8
17	7	$2s^23p\ ^2P_{1/2}$–$2s2p^2\ ^2D_{3/2}$	3.13×10^9	2.12×10^9
18	7	$2s^23p\ ^2P_{3/2}$–$2s2p^2\ ^2D_{3/2}$	3.11×10^8	2.09×10^8
12	8	$2p^3\ ^2D_{3/2}$–$2s2p^2\ ^2S_{1/2}$	2.95×10^6	1.87×10^6
14	8	$2p^3\ ^2P_{1/2}$–$2s2p^2\ ^2S_{1/2}$	5.69×10^8	6.12×10^8
15	8	$2p^3\ ^2P_{3/2}$–$2s2p^2\ ^2S_{1/2}$	7.62×10^8	7.53×10^8
17	8	$2s^23p\ ^2P_{1/2}$–$2s2p^2\ ^2S_{1/2}$	3.90×10^8	2.99×10^8
18	8	$2s^23p\ ^2P_{3/2}$–$2s2p^2\ ^2S_{1/2}$	4.06×10^8	3.13×10^8
12	9	$2p^3\ ^2D_{3/2}$–$2s2p^2\ ^2P_{1/2}$	4.23×10^8	4.35×10^8
14	9	$2p^3\ ^2P_{1/2}$–$2s2p^2\ ^2P_{1/2}$	1.61×10^9	1.61×10^9
15	9	$2p^3\ ^2P_{3/2}$–$2s2p^2\ ^2P_{1/2}$	3.10×10^8	3.24×10^8
17	9	$2s^23p\ ^2P_{1/2}$–$2s2p^2\ ^2P_{1/2}$	3.41×10^7	5.17×10^7

Table 2. (Continued.)

j	*i*	Transition	Present[a]	MCHF/MCDF Collection[b]
18	9	$2s^2 3p\ ^2P_{3/2}$–$2s2p^2\ ^2P_{1/2}$	2.10×10^6	6.93×10^6
11	10	$2p^3\ ^4S_{3/2}$–$2s2p^2\ ^2P_{3/2}$	1.09×10^4	1.27×10^4
12	10	$2p^3\ ^2D_{3/2}$–$2s2p^2\ ^2P_{3/2}$	7.61×10^7	7.70×10^7
13	10	$2p^3\ ^2D_{5/2}$–$2s2p^2\ ^2P_{3/2}$	4.87×10^8	4.97×10^8
14	10	$2p^3\ ^2P_{1/2}$–$2s2p^2\ ^2P_{3/2}$	7.30×10^8	7.41×10^8
15	10	$2p^3\ ^2P_{3/2}$–$2s2p^2\ ^2P_{3/2}$	1.90×10^9	1.93×10^9
17	10	$2s^2 3p\ ^2P_{1/2}$–$2s2p^2\ ^2P_{3/2}$	9.07×10^6	1.84×10^7
18	10	$2s^2 3p\ ^2P_{3/2}$–$2s2p^2\ ^2P_{3/2}$	2.97×10^7	5.45×10^7
19	12	$2s^2 3d\ ^2D_{3/2}$–$2s2p^2\ ^4P_{3/2}$	3.68×10^6	5.67×10^6
20	12	$2s^2 3d\ ^2D_{5/2}$–$2s2p^2\ ^4P_{3/2}$	2.21×10^5	4.80×10^5
19	13	$2s^2 3d\ ^2D_{3/2}$–$2p^3\ ^2D_{5/2}$	3.74×10^5	5.59×10^5
20	13	$2s^2 3d\ ^2D_{5/2}$–$2p^3\ ^2D_{5/2}$	3.74×10^6	5.74×10^5
16	14	$2s^2 3s\ ^2S_{1/2}$–$2p^3\ ^2P_{1/2}$	7.36×10^4	2.24×10^5
19	14	$2s^2 3d\ ^2D_{3/2}$–$2p^3\ ^2P_{1/2}$	2.00×10^6	2.84×10^5
16	15	$2s^2 3s\ ^2S_{1/2}$–$2p^3\ ^2P_{3/2}$	1.57×10^5	4.77×10^5
19	15	$2s^2 3d\ ^2D_{3/2}$–$2p^3\ ^2P_{3/2}$	3.96×10^5	4.99×10^5
20	15	$2s^2 3d\ ^2D_{5/2}$–$2p^3\ ^2P_{3/2}$	2.63×10^6	4.45×10^5
17	16	$2s^2 3p\ ^2P_{1/2}$–$2s^2 3s\ ^2S_{1/2}$	2.12×10^8	2.14×10^8
18	16	$2s^2 3p\ ^2P_{3/2}$–$2s^2 3s\ ^2S_{1/2}$	2.16×10^8	2.18×10^8
19	17	$2s^2 3d\ ^2D_{3/2}$–$2s^2 3p\ ^2P_{1/2}$	1.35×10^8	1.32×10^8
19	18	$2s^2 3d\ ^2D_{3/2}$–$2s^2 3p\ ^2P_{3/2}$	2.64×10^7	2.59×10^7
20	18	$2s^2 3d\ ^2D_{5/2}$–$2s^2 3p\ ^2P_{3/2}$	1.59×10^8	1.56×10^8

[a] Calculated using the same CI basis states that were employed to determine the energies in table 1.
[b] www.vuse.vanderbilt.edu/∼georgio/html_doc/header.html.

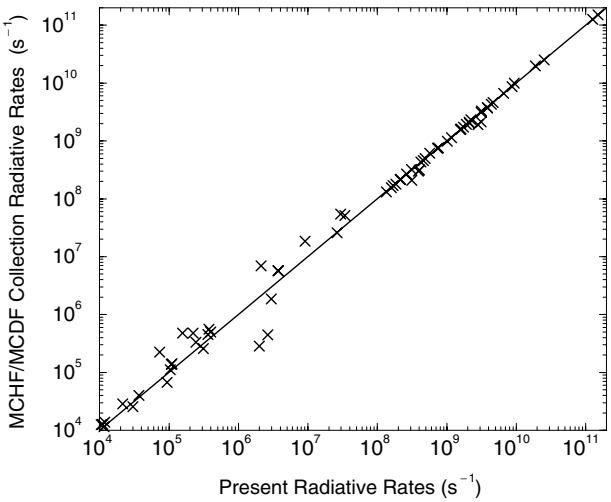

Figure 1. Graphical comparison of the present electric-dipole radiative rates with those from the MCHF/MCDF Collection.

the 180-level calculation. What is more difficult to see on the scale of this graph is that the additional coupling to the higher levels included in the 180-level calculation reduces the background cross sections. For example, for the $2s^2 2p\ ^2P_{3/2} \rightarrow 2s2p^2(^3P)\ ^4P_{3/2}$ transition at

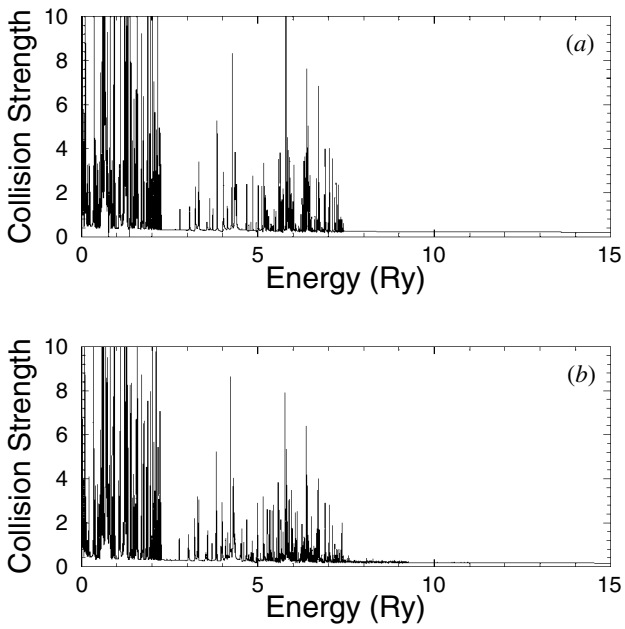

Figure 2. Collision strength for excitation from the $2s^2 2p\ ^2P_{1/2}$ ground level to the $2s^2 2p\ ^2P_{3/2}$ excited level. In (*a*) we show the results from the 20-level ICFT *R*-matrix calculation, while the curve in (*b*) is from the 180-level ICFT *R*-matrix calculation.

10.0 eV, the collision strength from the 180 level calculation is about 10% lower than that from the 20-level calculation.

In figure 4, we show the dipole-allowed transitions from both the $2s^2 2p\ ^2P_{1/2}$ ground level and the $2s^2 2p\ ^2P_{3/2}$ excited level to the $2s2p^2(^1D)\ ^2D_{3/2}$ level. Here the results are similar from both calculations, although the contributions from resonances are somewhat larger in the collision strengths from the 180-level calculation.

In table 3, we present the effective collision strengths for all possible transitions between the first seven levels in Ne^{5+} that are provided from the eight-term, 15-level calculation of Zhang *et al* [4]. We compare our 20-level and 180-level results with each other and those of Zhang *et al*. We see from the first entry in this table for the ground-term fine-structure transition that our 20-level results are below those of Zhang *et al* at the lowest temperature by about 33%, but are higher at the highest temperature by about 11%. The percentage differences between these results averaged over all temperatures is 12%. The 180-level results for this transition differ from the 20-level results by 10% at the lowest temperature, but by only 5% when averaged over all temperatures.

We also see from this table that the 180-level effective collision strengths for the transitions to the $2s2p^2(^3P)\ ^4P_{3/2}$ level from both the $2s^2 2p\ ^2P_{1/2}$ ground level and the $2s^2 2p\ ^2P_{3/2}$ excited level are below those of the 20-level calculation, except at the highest two temperatures. Thus, despite the added contributions from resonances included in the 180-level calculation, the effect of added coupling in the 180-level calculation is to reduce the effective collision strengths for these two transitions, except at higher temperatures. However, as we would expect from figure 4, the 180-level and 20-level effective collision strengths for the dipole-allowed transitions from the two ground-term levels to the $2s2p^2(^1D)\ ^2D_{3/2}$ level are in good agreement, differing by less than 3% when averaged over the temperatures.

Table 3. Effective collision strengths for all possible transitions between the first seven levels of Ne^{5+}. Here, c_1 and c_2 denote the $2s^22p$ and $2s2p^2$ configurations, respectively. For each transition, the first row is from Zhang *et al* [4]; the second row is from the present 11-term, 20-level ICFT calculation, and the third row is from the present 83-term, 180-level ICFT calculation.

	Electron temperature (K)						
Transition	1.25×10^4	5.00×10^4	1.00×10^5	2.50×10^5	5.00×10^5	7.50×10^5	1.25×10^6
$c_1\ ^2P_{1/2}$–$c_1\ ^2P_{3/2}$	3.05×10^0	2.14×10^0	1.96×10^0	1.48×10^0	1.03×10^0	8.11×10^{-1}	5.92×10^{-1}
	2.18×10^0	1.80×10^0	1.79×10^0	1.45×10^0	1.08×10^0	8.77×10^{-1}	6.61×10^{-1}
	2.42×10^0	1.75×10^0	1.70×10^0	1.38×10^0	1.03×10^0	8.44×10^{-1}	6.38×10^{-1}
$c_1\ ^2P_{1/2}$–$c_2\ ^4P_{1/2}$	8.56×10^{-2}	8.87×10^{-2}	7.88×10^{-2}	5.80×10^{-2}	4.63×10^{-2}	4.19×10^{-2}	3.67×10^{-2}
	1.23×10^{-1}	1.02×10^{-1}	9.02×10^{-2}	7.04×10^{-2}	5.62×10^{-2}	4.85×10^{-2}	3.94×10^{-2}
	1.13×10^{-1}	9.48×10^{-2}	8.39×10^{-2}	6.69×10^{-2}	5.55×10^{-2}	4.88×10^{-2}	4.01×10^{-2}
$c_1\ ^2P_{1/2}$–$c_2\ ^4P_{3/2}$	1.41×10^{-1}	1.43×10^{-1}	1.26×10^{-1}	9.00×10^{-2}	6.68×10^{-2}	5.68×10^{-2}	6.49×10^{-2}
	1.71×10^{-1}	1.58×10^{-1}	1.42×10^{-1}	1.09×10^{-1}	8.59×10^{-2}	7.35×10^{-2}	5.92×10^{-2}
	1.45×10^{-1}	1.44×10^{-1}	1.31×10^{-1}	1.04×10^{-1}	8.56×10^{-2}	7.49×10^{-2}	6.11×10^{-2}
$c_1\ ^2P_{1/2}$–$c_2\ ^4P_{5/2}$	1.34×10^{-1}	1.29×10^{-1}	1.10×10^{-1}	7.40×10^{-2}	5.14×10^{-2}	4.18×10^{-2}	3.26×10^{-2}
	1.25×10^{-1}	1.35×10^{-1}	1.20×10^{-1}	8.71×10^{-2}	6.42×10^{-2}	5.29×10^{-2}	4.08×10^{-2}
	1.13×10^{-1}	1.28×10^{-1}	1.14×10^{-1}	8.57×10^{-2}	6.76×10^{-2}	5.77×10^{-2}	4.56×10^{-2}
$c_1\ ^2P_{1/2}$–$c_2\ ^2D_{5/2}$	3.00×10^{-1}	3.05×10^{-1}	2.37×10^{-1}	1.47×10^{-1}	1.02×10^{-1}	8.34×10^{-2}	6.58×10^{-2}
	2.71×10^{-1}	2.80×10^{-1}	2.28×10^{-1}	1.57×10^{-1}	1.16×10^{-1}	9.64×10^{-2}	7.50×10^{-2}
	2.52×10^{-1}	2.55×10^{-1}	2.07×10^{-1}	1.50×10^{-1}	1.20×10^{-1}	1.03×10^{-1}	8.16×10^{-2}
$c_1\ ^2P_{1/2}$–$c_2\ ^2D_{3/2}$	1.18×10^0	1.16×10^0	1.11×10^0	1.13×10^0	1.25×10^0	1.35×10^0	1.52×10^0
	1.27×10^0	1.28×10^0	1.27×10^0	1.29×10^0	1.36×10^0	1.43×10^0	1.55×10^0
	1.22×10^0	1.23×10^0	1.23×10^0	1.27×10^0	1.35×10^0	1.42×10^0	1.53×10^0
$c_1\ ^2P_{3/2}$–$c_2\ ^4P_{1/2}$	9.45×10^{-2}	9.19×10^{-2}	7.89×10^{-2}	5.40×10^{-2}	3.88×10^{-2}	3.22×10^{-2}	2.55×10^{-2}
	1.23×10^{-1}	1.02×10^{-1}	8.80×10^{-2}	6.35×10^{-2}	4.70×10^{-2}	3.89×10^{-2}	3.03×10^{-2}
	1.09×10^{-1}	9.18×10^{-2}	7.99×10^{-2}	6.03×10^{-2}	4.81×10^{-2}	4.13×10^{-2}	3.29×10^{-2}
$c_1\ ^2P_{3/2}$–$c_2\ ^4P_{3/2}$	2.20×10^{-1}	2.18×10^{-1}	1.89×10^{-1}	1.31×10^{-1}	9.46×10^{-2}	7.89×10^{-2}	6.34×10^{-2}
	2.68×10^{-1}	2.36×10^{-1}	2.09×10^{-1}	1.56×10^{-1}	1.19×10^{-1}	1.01×10^{-1}	7.96×10^{-2}
	1.97×10^{-1}	2.03×10^{-1}	1.84×10^{-1}	1.45×10^{-1}	1.19×10^{-1}	1.03×10^{-1}	8.38×10^{-2}

Table 3. (Continued.)

	Electron temperature (K)						
Transition	1.25×10^4	5.00×10^4	1.00×10^5	2.50×10^5	5.00×10^5	7.50×10^5	1.25×10^6
$c_1\ ^2P_{3/2}$–$c_2\ ^4P_{5/2}$	4.06×10^{-1}	4.12×10^{-1}	3.62×10^{-1}	2.59×10^{-1}	1.94×10^{-1}	1.66×10^{-1}	1.37×10^{-1}
	3.99×10^{-1}	4.17×10^{-1}	3.81×10^{-1}	2.98×10^{-1}	2.36×10^{-1}	2.03×10^{-1}	1.64×10^{-1}
	3.46×10^{-1}	3.74×10^{-1}	3.43×10^{-1}	2.79×10^{-1}	2.34×10^{-1}	2.06×10^{-1}	1.69×10^{-1}
$c_1\ ^2P_{3/2}$–$c_2\ ^2D_{5/2}$	2.36×10^{0}	2.32×10^{0}	2.17×10^{0}	2.11×10^{0}	2.27×10^{0}	2.43×10^{0}	2.71×10^{0}
	2.47×10^{0}	2.53×10^{0}	2.47×10^{0}	2.44×10^{0}	2.53×10^{0}	2.63×10^{0}	2.82×10^{0}
	2.35×10^{0}	2.42×10^{0}	2.38×10^{0}	2.39×10^{0}	2.50×10^{0}	2.61×10^{0}	2.79×10^{0}
$c_1\ ^2P_{3/2}$–$c_2\ ^2D_{3/2}$	5.99×10^{-1}	6.02×10^{-1}	5.10×10^{-1}	4.07×10^{-1}	3.78×10^{-1}	3.79×10^{-1}	3.92×10^{-1}
	5.56×10^{-1}	5.82×10^{-1}	5.19×10^{-1}	4.35×10^{-1}	3.97×10^{-1}	3.86×10^{-1}	3.81×10^{-1}
	5.30×10^{-1}	5.56×10^{-1}	4.97×10^{-1}	4.30×10^{-1}	4.04×10^{-1}	3.94×10^{-1}	3.88×10^{-1}
$c_2\ ^4P_{1/2}$–$c_2\ ^4P_{3/2}$	5.96×10^{-1}	7.57×10^{-1}	7.40×10^{-1}	5.87×10^{-1}	4.44×10^{-1}	3.71×10^{-1}	2.92×10^{-1}
	5.43×10^{-1}	6.78×10^{-1}	6.89×10^{-1}	5.82×10^{-1}	4.59×10^{-1}	3.89×10^{-1}	3.08×10^{-1}
	5.07×10^{-1}	6.47×10^{-1}	6.57×10^{-1}	5.70×10^{-1}	4.76×10^{-1}	4.13×10^{-1}	3.32×10^{-1}
$c_2\ ^4P_{1/2}$–$c_2\ ^4P_{5/2}$	4.14×10^{-1}	5.39×10^{-1}	5.17×10^{-1}	4.01×10^{-1}	3.01×10^{-1}	2.55×10^{-1}	2.11×10^{-1}
	3.42×10^{-1}	5.02×10^{-1}	5.07×10^{-1}	4.17×10^{-1}	3.28×10^{-1}	2.82×10^{-1}	2.37×10^{-1}
	3.15×10^{-1}	4.75×10^{-1}	4.80×10^{-1}	4.05×10^{-1}	3.39×10^{-1}	3.00×10^{-1}	2.55×10^{-1}
$c_2\ ^4P_{1/2}$–$c_2\ ^2D_{5/2}$	1.67×10^{-1}	1.42×10^{-1}	1.26×10^{-1}	9.49×10^{-2}	7.28×10^{-2}	6.20×10^{-2}	5.01×10^{-2}
	1.32×10^{-1}	1.27×10^{-1}	1.20×10^{-1}	1.02×10^{-1}	8.47×10^{-2}	7.40×10^{-2}	6.02×10^{-2}
	1.19×10^{-1}	1.15×10^{-1}	1.09×10^{-1}	9.89×10^{-2}	8.90×10^{-2}	8.00×10^{-2}	6.60×10^{-2}
$c_2\ ^4P_{1/2}$–$c_2\ ^2D_{3/2}$	2.91×10^{-1}	2.22×10^{-1}	1.93×10^{-1}	1.46×10^{-1}	1.13×10^{-1}	9.66×10^{-2}	7.82×10^{-2}
	2.49×10^{-1}	2.11×10^{-1}	1.92×10^{-1}	1.62×10^{-1}	1.35×10^{-1}	1.18×10^{-1}	9.62×10^{-2}
	2.21×10^{-1}	1.91×10^{-1}	1.75×10^{-1}	1.55×10^{-1}	1.38×10^{-1}	1.23×10^{-1}	1.01×10^{-1}
$c_2\ ^4P_{3/2}$–$c_2\ ^4P_{5/2}$	1.17×10^{0}	1.51×10^{0}	1.46×10^{0}	1.15×10^{0}	8.68×10^{-1}	7.29×10^{-1}	5.86×10^{-1}
	9.84×10^{-1}	1.36×10^{0}	1.38×10^{0}	1.15×10^{0}	9.08×10^{-1}	7.75×10^{-1}	6.31×10^{-1}
	9.17×10^{-1}	1.30×10^{0}	1.32×10^{0}	1.13×10^{0}	9.41×10^{-1}	8.25×10^{-1}	6.81×10^{-1}

Table 3. (Continued.)

	Electron temperature (K)						
Transition	1.25×10^4	5.00×10^4	1.00×10^5	2.50×10^5	5.00×10^5	7.50×10^5	1.25×10^6
$c_2\,{}^4P_{3/2}$–$c_2\,{}^2D_{5/2}$	4.63×10^{-1}	3.75×10^{-1}	3.30×10^{-1}	2.49×10^{-1}	1.92×10^{-1}	1.64×10^{-1}	1.33×10^{-1}
	3.81×10^{-1}	3.47×10^{-1}	3.22×10^{-1}	2.73×10^{-1}	2.28×10^{-1}	1.99×10^{-1}	1.62×10^{-1}
	3.41×10^{-1}	3.15×10^{-1}	2.94×10^{-1}	2.64×10^{-1}	2.37×10^{-1}	2.13×10^{-1}	1.75×10^{-1}
$c_2\,{}^4P_{3/2}$–$c_2\,{}^2D_{3/2}$	4.53×10^{-1}	3.53×10^{-1}	3.07×10^{-1}	2.32×10^{-1}	1.79×10^{-1}	1.53×10^{-1}	1.24×10^{-1}
	3.82×10^{-1}	3.31×10^{-1}	3.03×10^{-1}	2.56×10^{-1}	2.13×10^{-1}	1.86×10^{-1}	1.52×10^{-1}
	3.41×10^{-1}	2.98×10^{-1}	2.75×10^{-1}	2.46×10^{-1}	2.19×10^{-1}	1.96×10^{-1}	1.61×10^{-1}
$c_2\,{}^4P_{5/2}$–$c_2\,{}^2D_{5/2}$	1.02×10^{0}	7.94×10^{-1}	6.91×10^{-1}	5.22×10^{-1}	4.04×10^{-1}	3.45×10^{-1}	2.79×10^{-1}
	8.63×10^{-1}	7.46×10^{-1}	6.80×10^{-1}	5.75×10^{-1}	4.80×10^{-1}	4.20×10^{-1}	3.41×10^{-1}
	7.69×10^{-1}	6.78×10^{-1}	6.25×10^{-1}	5.57×10^{-1}	4.96×10^{-1}	4.44×10^{-1}	3.65×10^{-1}
$c_2\,{}^4P_{5/2}$–$c_2\,{}^2D_{3/2}$	3.55×10^{-1}	2.99×10^{-1}	2.65×10^{-1}	2.00×10^{-1}	1.53×10^{-1}	1.31×10^{-1}	1.06×10^{-1}
	2.89×10^{-1}	2.70×10^{-1}	2.52×10^{-1}	2.15×10^{-1}	1.79×10^{-1}	1.57×10^{-1}	1.27×10^{-1}
	2.57×10^{-1}	2.45×10^{-1}	2.30×10^{-1}	2.09×10^{-1}	1.88×10^{-1}	1.69×10^{-1}	1.40×10^{-1}
$c_2\,{}^2D_{5/2}$–$c_2\,{}^2D_{3/2}$	4.20×10^{0}	2.39×10^{0}	1.82×10^{0}	1.16×10^{0}	7.73×10^{-1}	6.08×10^{-1}	4.55×10^{-1}
	2.50×10^{0}	1.81×10^{0}	1.48×10^{0}	1.01×10^{0}	7.04×10^{-1}	5.69×10^{-1}	4.25×10^{-1}
	2.38×10^{0}	1.71×10^{0}	1.40×10^{0}	1.01×10^{0}	7.66×10^{-1}	6.39×10^{-1}	4.98×10^{-1}

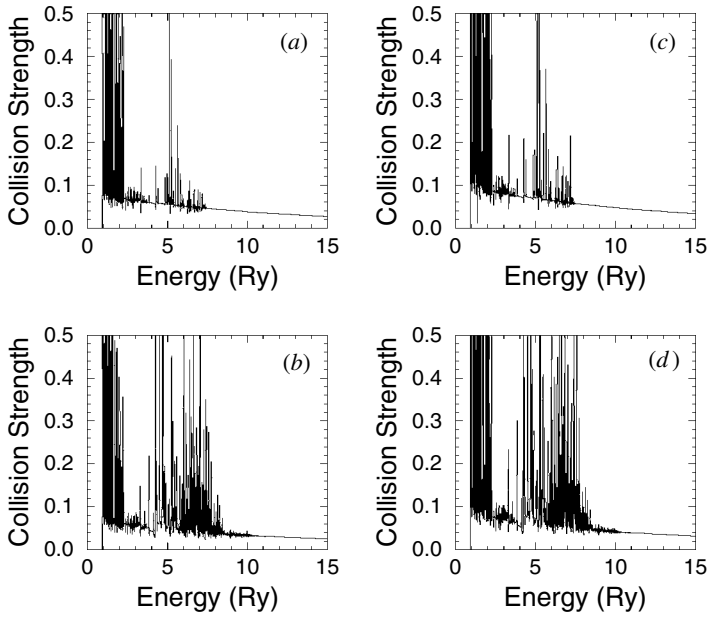

Figure 3. Collision strength for excitation from the levels of the $2s^22p$ configuration to the $2s2p^2(^3P)\ ^4P_{3/2}$ level. We show the results for the transition from the $2s^22p\ ^2P_{1/2}$ ground level from the 20-level ICFT calculation in (*a*) and from the 180-level ICFT calculation in (*b*). We show the collision strength for the transition from the $2s^22p\ ^2P_{3/2}$ excited level from the 20-level ICFT calculation in (*c*) and from the 180-level ICFT calculation in (*d*).

The overall agreement between the results of the 20-level calculation and those of Zhang *et al* is 13%, when averaged over all the temperatures and all the transitions given in table 3. On the other hand, the 180-level results differ from the 20-level results by only 6%, when averaged. This would indicate that either our 20-level calculation or the eight-term calculation of Zhang *et al* may be sufficiently accurate for transitions among the lowest seven levels. However, our comparison of the 180-level and 20-level results shows that there are much more substantial differences for transitions to and between the higher $n = 2$ and $2s^23\ell$ levels, especially at the lower temperatures. This should be expected, since there are substantial coupling effects to, and resonance contributions from, the levels that are included in our 180-level calculation and not our 20-level calculation. Thus, a detailed comparison of the effective collision strengths determined from our 20-level calculation with those determined from our 180-level calculation for transitions to and between the higher $n = 2$ and $2s^23\ell$ levels would not be meaningful.

The complete set of effective collision strengths for the 16 110 transitions between the 180 levels included in the present study up to a temperature of 2.5×10^6 K, along with reduced effective collision strengths at the infinite temperature limit and electric-dipole radiative rates, all tabulated in the ADAS *adf04* format [21], are available via the WWW under http://www-cfadc.phy.ornl.gov/data_and_codes.

It is always difficult to estimate the accuracy of large-scale calculations of electron-impact excitation, since the uncertainties vary dramatically from one type of transition to another. Nevertheless, some general statements can be made. We would expect that the effective collision strengths for strong dipole-allowed transitions, which normally are not affected significantly by resonance contributions, should be good to about 20%. The accuracy of the collision strengths for dipole-forbidden or weakly-allowed dipole transitions is much more

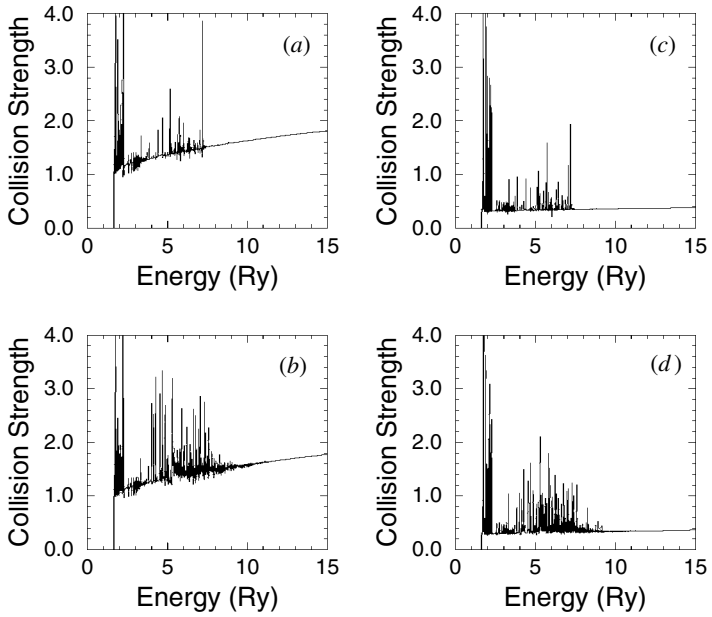

Figure 4. Collision strength for excitation from the levels of the $2s^2 2p$ configuration to the $2s2p^2(^1D)\ ^2D_{3/2}$ level. We show the results for the transition from the $2s^2 2p\ ^2P_{1/2}$ ground level from the 20-level ICFT calculation in (*a*) and from the 180-level ICFT calculation in (*b*). We show the collision strength for the transition from the $2s^2 2p\ ^2P_{3/2}$ excited level from the 20-level ICFT calculation in (*c*) and from the 180-level ICFT calculation in (*d*).

difficulty to estimate. Such transitions are often dominated by resonance contributions and this introduces more uncertainty into the effective collision strengths. However, the tests we have made on our energy mesh would indicate that it resolved the dominant resonances and this will decrease the uncertainty in these contributions. In addition, the strong dipole transitions have relatively small contributions from the dipole top-up, indicating that the sum over partial waves is nearly converged. This is not true of the weak-dipole transitions, since a large fraction of them had dipole top-up contributions of more than 30%.

It should also be noted that, even for strong-dipole transitions, the effective collision strengths for excitation to and between the upper levels should be considered somewhat less accurate. This is partially due to the fact that above the $2p^2(^3P)3p\ ^4S_{3/2}$ level (level 95 in table 1), levels arising from configurations with $n \geqslant 5$ begin to appear. Coupling to these states and resonance contributions arising from them, which are not included here, will become more important for excitation to and between these upper levels. Finally, coupling to the target continuum has been shown to reduce the collision strengths for transition to the upper levels in simple species [22–24]. Such coupling effects are not included here, but these effects should be relatively small in a five times ionized species [24].

5. Conclusions

We have performed 20-level and 180-level intermediate-coupling frame-transformation *R*-matrix coupling calculations for Ne^{5+}. The electric-dipole radiative rates determined from our large CI Breit–Pauli calculation are in good agreement with unpublished rates available from the MCHF/MCDF Collection on the WWW. Our effective collision strengths from both

calculations are consistent with the earlier calculations of Zhang *et al* [4]. The agreement between our 20-level and 180-level results for the lower-energy transitions is quite good; this indicates that if one is only interested in transitions among the lowest seven $n = 2$ levels or so, that our 20-level calculation, or even the smaller calculation of Zhang *et al* [4], is sufficient. However, in order to do accurate collisional–radiative modelling for this ion, a much more complete set of collisional data is required, and that is provided by our 180-level calculation. Furthermore, such large calculations for other atomic species are now much more practical with the implementation of the parallel versions of the ICFT R-matrix codes. The complete set of radiative rates from our Breit–Pauli calculation and effective collision strengths from our 180-level ICFT R-matrix calculation are available on the WWW at the CFADC site at ORNL.

Acknowledgments

In this work, DMM was supported by a subcontract with Los Alamos National Laboratory, DCG was supported by a US DoE Grant (DE-FG02-96-ER54367) with Rollins College, and NRB was supported by a UK PPARC grant (PPA/G/S/1997/00783) with the University of Strathclyde.

References

[1] Griffin D C and Badnell N R 2000 *J. Phys. B: At. Mol. Opt. Phys.* **33** 4389
[2] Griffin D C, Mitnik D M and Badnell N R 2001 *J. Phys. B: At. Mol. Opt. Phys.* **34** 4401
[3] Hayes M A 1992 *J. Phys. B: At. Mol. Opt. Phys.* **25** 2649
[4] Zhang H L, Graziani M and Pradhan A K 1994 *Astron. Astrophys.* **283** 28
[5] Griffin D C, Badnell N R and Pindzola M S 1998 *J. Phys. B: At. Mol. Opt. Phys.* **31** 3713
[6] Gorczyca T W and Badnell N R 2000 *J. Phys. B: At. Mol. Opt. Phys.* **33** 2511
[7] Saraph H E 1978 *Comput. Phys. Commun.* **15** 247
[8] Griffin D C, Badnell N R, Pindzola M S and Shaw J A 1999 *J. Phys. B: At. Mol. Opt. Phys.* **32** 2139
[9] Berrington K A, Eissner W B and Norrington P H 1995 *Comput. Phys. Commun.* **92** 290
[10] Snir M, Otto S W, Huss-Lederman S, Walker D W and Dongarra J J 1996 *MPI: the Complete Reference* (Cambridge, MA: MIT Press)
[11] Blackford L S *et al* 1997 *ScaLAPACK User's Guide* (Philadelphia, PA: SIAM)
[12] Gorczyca T W, Robicheaux F, Pindzola M S, Griffin D C and Badnell N R 1995 *Phys. Rev.* A **52** 3877
[13] Badnell N R, Gorczyca T W and Price A D 1998 *J. Phys. B: At. Mol. Opt. Phys.* **31** L239
[14] Froese Fischer C 1991 *Comput. Phys. Commun.* **64** 369
[15] Burgess A 1974 *J. Phys. B: At. Mol. Phys.* **7** L364
[16] Burgess A, Hummer D G and Tully J A 1970 *Phil. Trans. R. Soc.* A **266** 225
[17] Seaton M J 1953 *Proc. R. Soc.* A **218** 400
[18] Burgess A and Tully J A 1992 *Astron. Astrophys.* **254** 436
[19] Whiteford A D, Badnell N R, Ballance C P, O'Mullane M G, Summers H P and Thomas A L 2001 *J. Phys. B: At. Mol. Opt. Phys.* **34** 3179
[20] Kelly R L 1987 *J. Phys. Chem. Ref. Data* **16** (Suppl.1)
[21] Summers H P 1999 *ADAS User Manual Version 2.1* webpage http://adas.phys.strath.ac.uk/
[22] Bartschat K, Hudson E T, Scott M P, Burke P G and Burke V M 1996 *J. Phys. B: At. Mol. Opt. Phys.* **29** 115
[23] Bartschat K and Bray I 1997 *J. Phys. B: At. Mol. Opt. Phys.* **30** L109
[24] Griffin D C, Badnell N R and Pindzola M S 2000 *J. Phys. B: At. Mol. Opt. Phys.* **33** 1013